

Supporting Information for:

**Active Control of Multiple, Simultaneous Nonlinear Optical
Processes in Plasmonic Nanogap Cavities**

Qixin Shen,¹ Weiliang Jin,² Guoce Yang,^{3,4} Alejandro W. Rodriguez,² Maiken H. Mikkelsen^{3,}*

¹Department of Physics, Duke University, Durham, North Carolina 27708, USA

²Department of Electrical Engineering, Princeton University, Princeton, New Jersey 08544, USA

³Department of Electrical and Computer Engineering, Duke University, Durham, North Carolina
27708, USA

⁴State Key Laboratory of Precision Measurement Technology and Instruments, Department of
Precision Instrument, Tsinghua University, Beijing 100084, China

*Correspondence to: m.mikkelsen@duke.edu, +1 (919) 660-0185

Fabrication details

The samples used in this work were fabricated by first depositing a 75 nm gold film onto a silicon substrate by electron-beam evaporation with 2 Å/s deposition rate. Then, an ultrathin dielectric Al₂O₃ layer was deposited on top of the gold film by atomic layer deposition (ALD) by VaporPulse Technologies, Inc and the thicknesses were confirmed by ellipsometry measurements. Finally, electron-beam lithography (EBL) was used to fabricate silver nanorectangles on top of the dielectric layer with a height of 30 nm. Different rectangle widths and lengths were fabricated on each sample to ensure that the resulting plasmon resonances could be matched with the two excitation wavelengths. The structural dimensions were measured by scanning electron microscopy (SEM).

Optical setup

As shown in the Figure S1, the samples were excited by a Ti: sapphire laser (Coherent Chameleon, ~200 fs pulse duration, 80 MHz repetition rate) and an optical parametric oscillator pumped by the same Ti: sapphire laser. Half-wave plates were used to control the polarization state of these two excitations and a variable delay line was used to control the relative time difference between the two laser pulses. The two laser pulses were then combined by a beam splitter and focused onto the sample plane via a microscope objective (Mitutoyo M Plan Apo NIR, 50×). The same objective was used to collect the nonlinear signals in a reflection geometry, which were then passed through a dichroic mirror and a short-pass filter (600 nm) before being detected by a CCD-coupled (Princeton Instruments 400 BR Excelon) spectrometer (Acton sp2500i). A white light imaging system was also incorporated into the setup for bright field imaging.

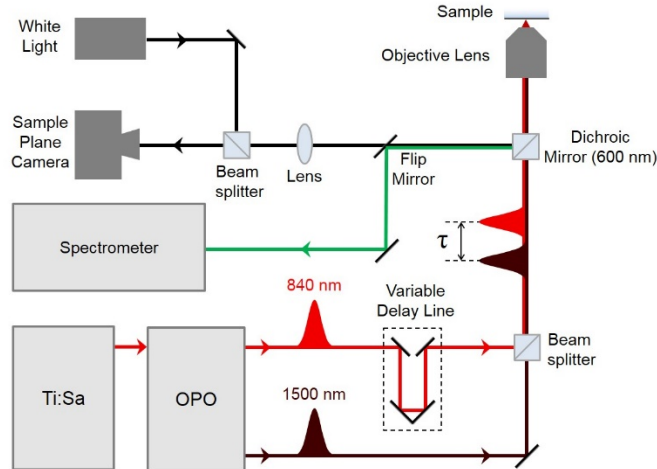


Figure S1. Schematic of optical setup.

Control experiments of Al_2O_3 on gold film

The intensities of the nonlinear signal from different thicknesses of Al_2O_3 on the gold film were measured as references to extract the enhancement factors of the silver nanorectangle structures discussed in the main text. A bare gold film was also included as a reference. As shown in Figure S2, the THG and FWM intensities remain constant, while the SFG intensities increase slightly with thicker Al_2O_3 layer. This is likely due to further breaking of inversion symmetry from the Al_2O_3 layer and gold ground plane interface since SFG is a second order nonlinear optical process.

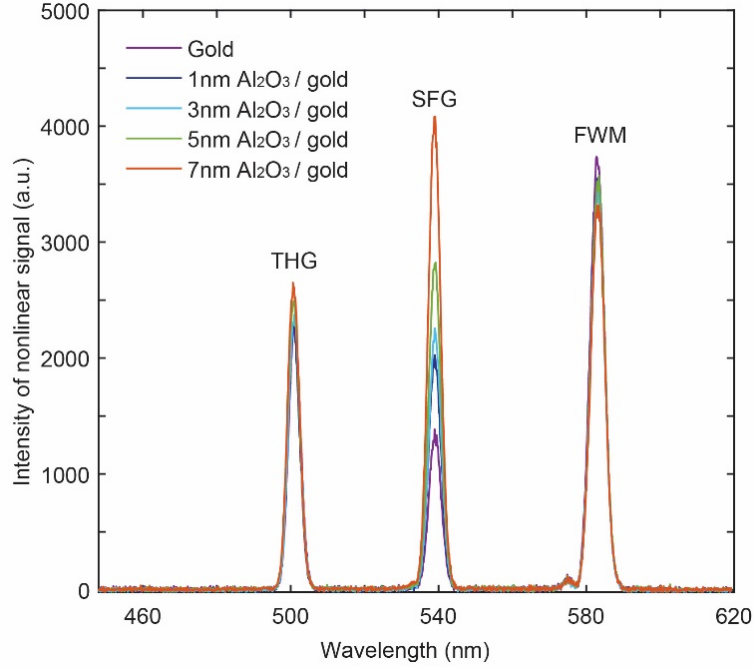


Figure S2. Intensities of the nonlinear signal from third harmonic generation (THG), sum frequency generation (SFG) and four wave mixing (FWM) for different thicknesses of Al₂O₃ on a gold film (without nanorectangles) and a bare gold film for reference.

Theoretical analysis

To quantify the three nonlinear processes where the modal amplification only occur at the pumping frequencies, we begin by applying coupled mode analysis to determine the mode amplitude $a_{1(2)}$ when a laser beam of power $P_{1(2)}$ is supplied to excite the mode at $\omega_{1(2)}$. In the non-depleted region where down-conversion is negligible, and assuming a mode is predominant at $\omega_{1(2)}$, the modes at $\omega_{1(2)}$ are decoupled, leading to a simple expression $a_i = \mathcal{L}(\Delta\omega_i)\sqrt{P_i}$, where the

subscript $i = 1(2)$ denotes quantities at $\omega_{1(2)}$, $\mathcal{L}(\Delta\omega_i) = \frac{\sqrt{\gamma_{ri}}}{\gamma_i + i\Delta\omega_i}$ a Lorentzian function depending

on the frequency detuning from the resonant frequency $\Delta\omega_i = \omega - \omega_i$, and the radiative (total) decay rate of the respective resonance $\gamma_{ri}(\gamma_i)$.

The nonlinear polarization $\mathcal{P}(\mathbf{r})$ at the output frequency can be expressed in terms of the fields at ω_i , which is a product of a_i and the normalized modal profile $\mathbf{E}_i(\mathbf{r})$,

$$\mathcal{P}(\mathbf{r}, \omega = \sum_{i=1}^n c_i \omega_i) = \varepsilon_0 \left[\overline{\overline{\chi^{(n)}}} \prod_{i=1}^n a_i^{c_i(*)} \mathbf{E}_i^{c_i(*)}(\mathbf{r}) \right] \quad (\text{S1})$$

where the $(n+1)$ th-rank tensor $\overline{\overline{\chi^{(n)}}}$ is the n th-order nonlinear susceptibility, $c_i = 1(-1)$ for positive (negative) frequency, and $c_i(*)$ denotes complex conjugation for $c_i = -1$ and no conjugation otherwise. With eq S1, while the detailed electric field profile at the output frequency can be evaluated by solving the linear Maxwell's equations, the scaling of the output power with respect to P_i and $\Delta\omega_i$ can be written analytically, as they only appear in the prefactor a_i in eq S1.

Simulations of the electric field distribution and nonlinear power generation

A three dimensional frequency-domain finite-element method (COMSOL Multiphysics) was used to simulate the nonlinear frequency conversion processes in our nanorectangle structures. The dimensions used in the simulation are from the experimental design and are confirmed by SEM and ellipsometry measurements. Note that the silver nanorectangles do not have sharp corners in our fabrication, thus we round the edges of the silver nanorectangle structures by 8 nm radius according to our SEM measurement. Along the incidence direction, perfectly matched layer (PML) of thickness 250 nm is added at the top and the bottom of the entire domain; while along the other two dimensions, periodic boundary conditions were applied. To compute the nonlinear

power generation, while in principle one needs to solve a set of nonlinear equations, we notice that all the three nonlinear processes in our experiment are in the weak signal region, as confirmed in Figure 2 of the main text, enabling us to solve instead few coupled linear Maxwell equations. More specifically, we divide our simulation into two steps: (i) At each pumping frequency, we solve for the electric field profiles regarding a normal incident plane wave with an appropriate polarization onto the structures. The resonance frequency can be obtained from the reflection spectra, generated via a frequency sweep. We have illustrated the electric field distributions of the longitudinal and transverse gap plasmon mode in Figure 1 and Figure 4 of the main text. (ii) Given the electric field profiles at the pumping frequencies, we assemble the nonlinear polarizations, and include them as an external volume current source at the output frequency. More specifically, for each nonlinear process, assuming all the nonlinear materials to be isotropic (the thin Al₂O₃ layer can be regarded as amorphous), the nonlinear polarization is defined as follows:

$$\begin{aligned}
\mathbf{P}^{SFG} &= \varepsilon_0 \overline{\chi^{(2)}} \mathbf{E}(\omega_1) \mathbf{E}(\omega_2) \\
\mathbf{P}^{THG} &= \varepsilon_0 \chi^{(3)} [\mathbf{E}(\omega_2) \cdot \mathbf{E}(\omega_2)] \mathbf{E}(\omega_2) \\
\mathbf{P}^{FWM} &= \frac{1}{3} \varepsilon_0 \chi^{(3)} \left[\begin{aligned} &(\mathbf{E}(\omega_1) \cdot \mathbf{E}(\omega_1)) \mathbf{E}^*(\omega_2) + \\ &2(\mathbf{E}(\omega_1) \cdot \mathbf{E}^*(\omega_2)) \mathbf{E}(\omega_1) \end{aligned} \right]
\end{aligned} \tag{S2}$$

where we have expressed $\chi^{(3)}$ tensor explicitly for isotropic media, while the surface $\chi^{(2)}$ tensor on an isotropic surface is more complicated, whose components can be classified into three families.¹ For simplicity, we assume that the $\chi^{(2)}$ values of the three families are equal (we find that in the gap plasmon, the contribution from $\chi_{zzz}^{(2)}$ of Al₂O₃ dominates, making other components less relevant), and $\chi^{(2)}$ is only nonzero in a layer of finite thickness near the interface. Table S1 summarizes the values of $\chi^{(2)}$ and $\chi^{(3)}$ used in our simulation.^{1,2} We then solve for the field profile

at the output frequency, with which the nonlinear power can be computed by integrating the Poynting flux across the output port.

Table S1. $\chi^{(2)}$ and $\chi^{(3)}$ values used in simulation.

	Gold	Silver	Al ₂ O ₃
$\chi^{(2)}$ (m/V)	1.47×10^{-12}	0.95×10^{-12}	0.30×10^{-12}
$\chi^{(3)}$ (m ² /V ²)	7.60×10^{-19}	2.80×10^{-19}	3.10×10^{-22}

References

- (1) Krause, D.; Teplin, C. W.; Rogers, C. T. Optical Surface Second Harmonic Measurements of Isotropic Thin-Film Metals: Gold, Silver, Copper, Aluminum, and Tantalum. *J. Appl. Phys.* **2004**, *96* (7), 3626–3634.
- (2) Boyd, R. W. *Nonlinear Opt.*, 3rd ed.; Academic Press: San Diego, 2008.